Geophysical Prospecting
EAGE EUROPEAN ASSOCIATION OF GEOSCIENTISTS & ENGINEERS
Geophysical Prospecting, 2021, **69**, 1034–1054 doi: 10.1111/1365-2478.13090

Cable reverberations during wireline distributed acoustic sensing measurements: their nature and methods for elimination

Evgeniia Martuganova[1,2]*, Manfred Stiller[1], Klaus Bauer[1], Jan Henninges[1] and Charlotte M. Krawczyk[1,2]

[1]*GFZ German Research Centre for Geosciences, Potsdam, Germany, and* [2]*Technical University Berlin, Institute of Applied Geosciences, Berlin, Germany*

Received April 2020, revision accepted March 2021

ABSTRACT

The application of distributed acoustic sensing in borehole measurements allows for the use of fibre optic cables to measure strain. This is more efficient in terms of time and costs compared with the deploying of conventional borehole seismometers. Nevertheless, one known drawback for temporary deployment is represented by the freely hanging wireline cable slapping and ringing inside the casing, which introduces additional coherent coupling noise to the data. The present study proposes an explanation for the mechanism of noise generation and draws an analogy with similar wave propagation processes and phenomena, such as ghost waves in marine seismics. This observation allows to derive a ringing noise filter function, to study its behaviour and to consider known effects of the gauge length filter. After examining existing methods aimed at eliminating ringing noise and results of their application, we propose a two-step approach: (1) developing a denoising method based on a matching pursuit decomposition with Gabor atoms and (2) subtracting the noise model for imaging improvement. The matching pursuit method focuses on decomposing the original input signal into a weighted sum of Gabor functions. Analysing Gabor atoms properties for frequency, amplitude and position in time provides the opportunity to distinguish parts of the original signal denoting noise caused by the vibrating cable. The matching pursuit decomposition applied to the distributed acoustic sensing-vertical seismic profiling data at the geothermal test site Groß Schönebeck provides a versatile processing instrument for noise suppression.

Key words: Borehole geophysics, Distributed acoustic sensing, Noise, Signal processing, Vertical seismic profiling.

INTRODUCTION

During the last decade, distributed acoustic sensing (DAS), a technology of seismic data acquisition using fibre optic cable as a linearly arranged array of sensors, has gained a wide range of application in geoscience (Dou *et al.*, 2017; Henninges *et al.*, 2017; Jousset *et al.*, 2018; Mondanos and Coleman, 2019; Kobayashi *et al.*, 2020; Naldrett *et al.*, 2020). In comparison with classical vertical seismic profiling (VSP), DAS technology application allows recording a continuous data set faster and more cost effectively. Currently, the majority of surveys are obtained using fibre optic cables permanently installed behind the casing or along the tubing (Mateeva *et al.*, 2014; Correa *et al.*, 2017; Grandi, Dean and Tucker, 2017; Götz *et al.*, 2018). However, there are a significant number of drilled wells in which only the use of wireline DAS technology is possible. Nevertheless, only a limited amount of data examples recorded using temporarily installed wireline cable

*E-mail: evgeniia.martuganova@gfz-potsdam.de

are available (Hartog *et al*., 2014; Borland, Hearn and Sayed, 2016; Yu *et al*., 2016a; Yu *et al*., 2016b; Willis *et al*., 2019).

One of the possible explanations to this fact might be that the temporary cable installation causes problems with proper cable coupling and, as a result, it increases additional coherent noise in the data.

Miller *et al*. (2012) showed for the first-time data acquired using a temporarily installed fibre optic cable at Devine test site near San Antonio, Texas. The ringing signals are present in the shallow depths for all source positions and were explained as a poor coupling effect. For noise suppression a single-channel notch filter and orthogonal projection operators were applied.

Later, several authors encounter the same noise patterns during DAS data recording using wireline installation (Hartog *et al*., 2014; Dean *et al*., 2015; Yu *et al*., 2016a). Schilke *et al*. (2016) and Constantinou *et al*. (2016) raised the idea of providing slack to the cable during data recording to improve cable coupling to borehole walls. It was studied using numerical modelling methods and field tests from Rittershoffen, France. However, the demonstrated data set example acquired with recommended 2% slack showed a reduced amount of the noise as well as decrease of the signal-to-noise ratio in the region of cable accumulation.

Barberan *et al*. (2012), Didraga (2015) and Daley *et al*. (2016) report on ringing noise zones in the data acquired using a DAS cable clamped to the tubing. According to Didraga (2015), a noise generation mechanism is associated with vertical sections of the boreholes in which the tubing acts like a vibrating string between the contact points with an outer casing. Daley *et al*. (2016) explain ringing noise events as reverberation waves trapped between two depths. Also, the above authors suggest noisy regions in the data corresponding to wave propagation in a poorly cemented steel casing.

Willis *et al*. (2019) further explored the properties of the ringing noise and described different velocities of up- and downgoing part of the zigzags of the noise. The noise generation is interpreted as a back-and-forth reverberation in depth regions of a loose cable.

Given this variability, the comprehension of the noise nature and the physical mechanism of its origin is essential for the subsequent imaging quality improvement. In this study, we add to the available approaches. For this purpose, we propose a physical model of so-called ringing noise and a means for its elimination based on a matching pursuit decomposition (MPD) with Gabor atoms. We evidence this by a case study at the Groß Schönebeck site, Germany.

DISTRIBUTED ACOUSTIC SENSING-VERTICAL SEISMIC PROFILING EXPERIMENT

The Groß Schönebeck research platform operated by the German Research Centre for Geosciences (GFZ) is located 40 kilometres northeast of Berlin on the southern edge of the North German Basin. It serves as a reference site for geothermal energy technology development for sustainable energy production from low permeability deep geothermal reservoirs. The target geothermal reservoir zone at depths of 4000 to 4300 m is represented by siliciclastic sediments and volcanic rocks of Lower Permian (Rotliegend) age, overlaid by Zechstein salt (Zimmermann, Moeck and Blöcher, 2010).

A distributed acoustic sensing (DAS) vertical seismic profiling (VSP) data set was acquired at the Groß Schönebeck *in situ* geothermal laboratory in February 2017 (Henninges *et al*., 2021) with the additional intent to support the high-resolution 3D reflection seismic survey from the surface (Stiller *et al*., 2018). The 3D seismic survey, covering an area of 8 km by 8 km, has its focus on reservoir depths at 4 km. The main goal of the 3D seismic survey was to enhance the comprehension of the geological structures and to reveal the spatial configuration of fault structures (Krawczyk *et al*., 2019; Bauer *et al*., 2020).

The VSP experiment, in its turn, was designed to enable detailed imaging around the existing boreholes and especially to additionally improve 3D surface seismic interpretation in the reservoir target area.

Acquisition parameters

Two wireline, hybrid cables (electrical and optical; from SLB (NOVA-F) and GFZ (Rochester) (Henninges *et al*., 2011)) were temporarily installed in the 4.3 km deep wells E GrSk 3/90 (maximum inclination 7.2°) and Gt GrSk 4/05 (maximum inclination 49°) (Fig. 1). The DAS sensor cable was freely lowered inside the water-filled borehole until maximum measured depth in E GrSk 3/90 (4309 m measured depth (MD)), and in Gt GrSk 4/05 it was deployed until an existing restriction (4214.17 m MD). Data were recorded on single-mode fibres using hDVS (the heterodyne distributed vibration sensing, Schlumberger) technology. The spatial sampling along the borehole was set to 5 m. The recorded physical quantity of the fibre optic DAS/hDVS system is strain, distributed over a gauge length (a section of the fibre over which the strain is measured). Data were recorded using 20-m gauge length but later adjusted to processing optimized 40 m to achieve a

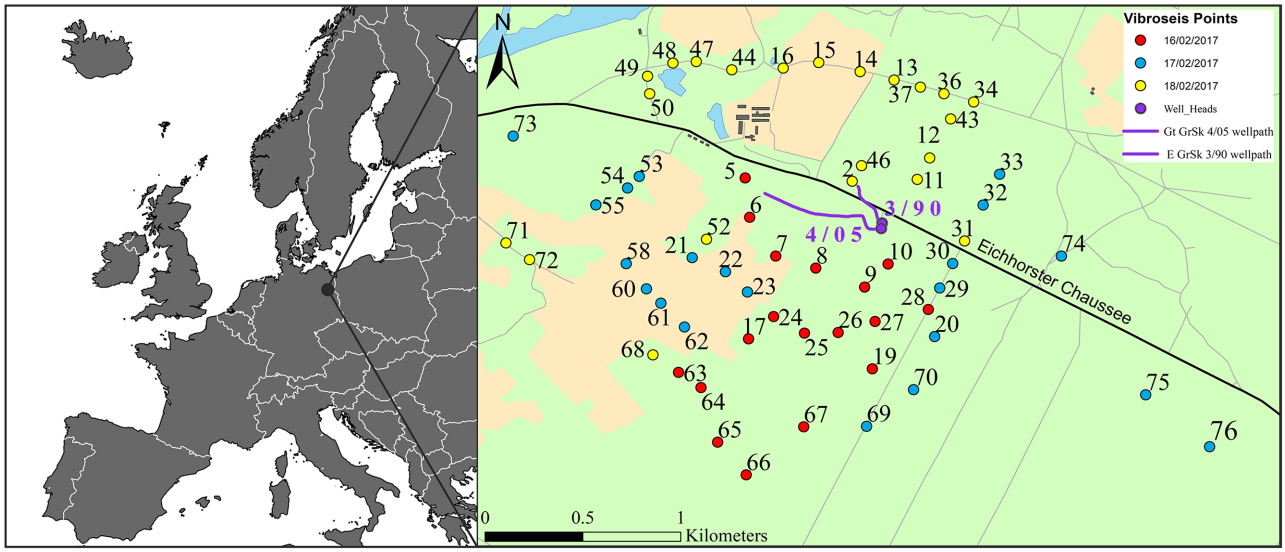

Figure 1 Location of the Groß Schönebeck geothermal site. Left: Position in the Northeast German basin in Europe. Right: Base map of the Groß Schönebeck geothermal site with two boreholes (violet circles) in the centre and 61 VSP source points arranged in a spiral pattern around. Borehole trajectories are shown in violet. VP locations are shown in different colours corresponding to the day of acquisition: 18 VPs on day −1 (red dots), 18 VPs on day −2 (blue dots) and 25 VPs on day −3 (yellow dots).

compromise between S/N maximization and loss of the signal frequencies (see also Dean, Cuny and Hartog, 2017, for further debate). During the experiment, we had 61 vibroseis points (VP), located at different offsets (from 200 to 2000 m) and azimuths, forming a spiral around the boreholes (Fig. 1). Four heavy trucks vibrated simultaneously and repeatedly at each VP location, with an average stacking fold of 16 per source location. For the data acquisition, a linear sweep of 10–112 Hz and 36 s length was used. For several VPs with larger offsets, we used a sweep from 10 to 96 Hz. Overall, the VSP experiment measurements were conducted during four acquisition days (one day for detailed pre-survey start-up tests and three days of data acquisition). More experiment planning and data acquisition details can be found in Henninges *et al.* (2021).

We performed different noise analysis and denoising tests on the vertically stacked raw DAS strain data set recorded at source position 10 (Fig. 1) in well Gt GrSk 4/05 during pre-survey tests with 26 sweep repetitions with 1 m slack applied to the cable. This choice was dictated by the availability of independent measurements with the versatile seismic imager (VSI) tool string recorded in the same well with the same sweep parameters 10–88 Hz and 36 s length. A direct comparison of conventional acceleration point sensor measurements and denoising results allows to get a better understanding of DAS data and to perform additional quality control of the proposed denoising processing workflow so that these data serve as a reference for the DAS data processing. Checkshots were recorded at 1200, 2400, 3600 and 4207 m MD.

RINGING NOISE

Yu *et al.* (2016a) and Willis *et al.* (2019) present examples of distributed acoustic sensing (DAS) data sets recorded on a wireline cable. The authors pose that such ringing noise is most likely caused by poor coupling of the sensor cable and the borehole casing, which is visible in certain depth intervals. During wireline acquisition, the cable is not fixed and hangs freely inside the borehole; thus, cable coupling inside the well is not well controllable. Due to a borehole's conditions, such as inclination and completion at specific depth ranges, the cable contact with the borehole wall varies; therefore, some areas are likely subjected to reverberations caused by different sources such as a vibroseis signal during data acquisition (Yu *et al.*, 2016a; Willis *et al.*, 2019). Cable slapping creates a specific noise pattern, elimination of which leads to considerable complication during data processing.

A typical DAS vertical seismic profiling (VSP) section from Groß Schönebeck (Fig. 2a) presents this ringing noise phenomenon, as described above. The recorded seismic data show narrow-band noise trains with a stripe or characteristic zigzag patterns in the time domain (Fig. 2b) over at least 19 different depth regions, for instance at 594–849, 1548–1702, 2984–3282 and 3735–3807 m measured depth (Fig. 2a). We

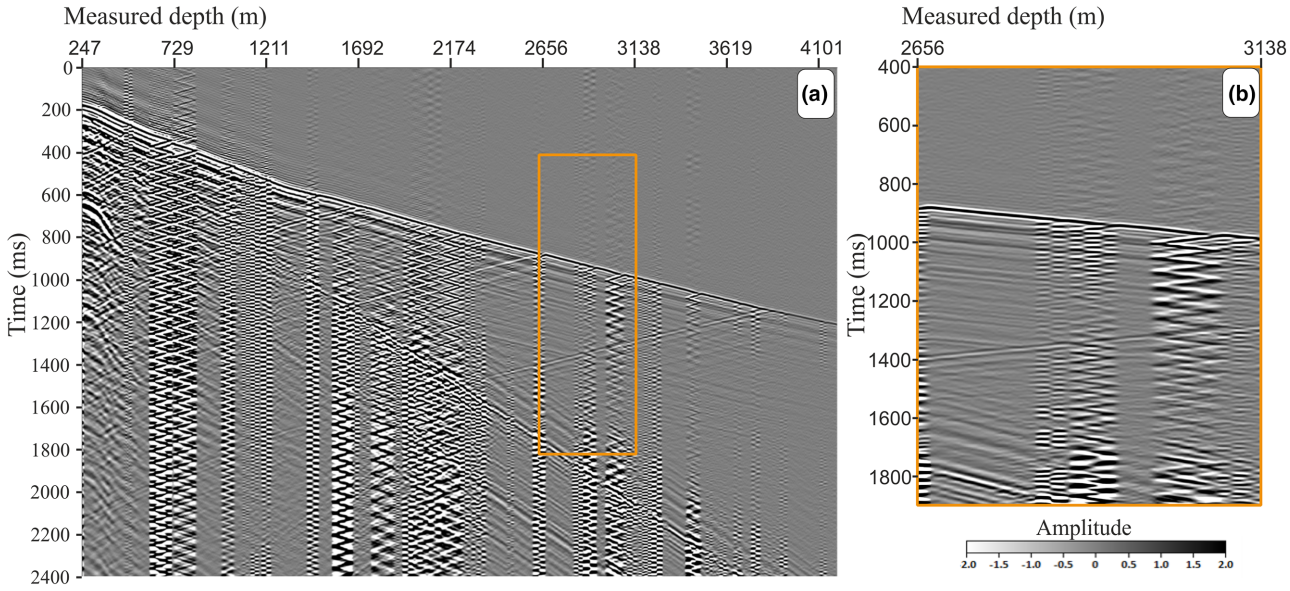

Figure 2 Example of a typical DAS VSP section from Groß Schönebeck. (a) Common source gather contaminated with noise, recorded for VP10 after preprocessing (vertical stacking, correlation with the pilot sweep and subsequent differentiation to achieve acceleration-like characteristics; seismic software ProMAX R5000, Halliburton). (b) The orange rectangle shows zoomed fragment of the seismic section for the depth range 2656–3138 m.

refer to this type of noise as ringing noise. In the time domain, the noisy intervals often follow one after another, forming a larger noisy zone and even overlap like in depth interval 1755–2367 m. These zigzag patterns obscure important features such as reflections.

In the frequency domain (Fig. 3), high-amplitude peaks in the amplitude spectrum can be observed. The white arrows illustrate periodic maximums corresponding to 18 Hz frequency multiples (i.e. 18, 36, 54 Hz etc.) for the seismic trace at 622.76 m MD. A similar pattern of the high-amplitude values, occurring with a certain periodicity, is also noticeable at different depth levels. The amplitude values of the peaks vary for each of the different depth levels and frequency values. Unlike in time domain displays, frequency domain displays allow for a better separation of the individual zigzag intervals and provide a better understanding of the noise. It appears that the shallow part of the record contains more noisy intervals in comparison with the deeper part (below 2000 m). From one VP record to another, these affected depth regions do not change significantly in the study presented. If we compare depth section 1418–1490 m with depth section 1760–1909 m, we can recognize that both depth intervals contain coherent noise. However, there is a distinct difference in the level of noise contamination. Furthermore, seismic data recorded, for instance, in section 2670–2820 m, show no signs of ringing noise at all. Possibly, these differences in local amplitude and

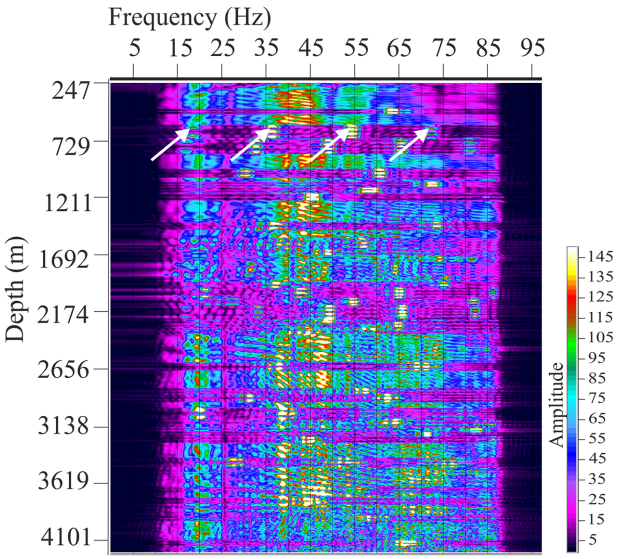

Figure 3 FX amplitude spectra of the VP10 seismic section after preprocessing. Irregularly occurring maximums correspond to resonances. White arrows highlight examples of the ringing noise occurrence.

S/N ratio occur due to variable coupling conditions. Ringing noise generation mechanism will be further investigated in the next section of the paper.

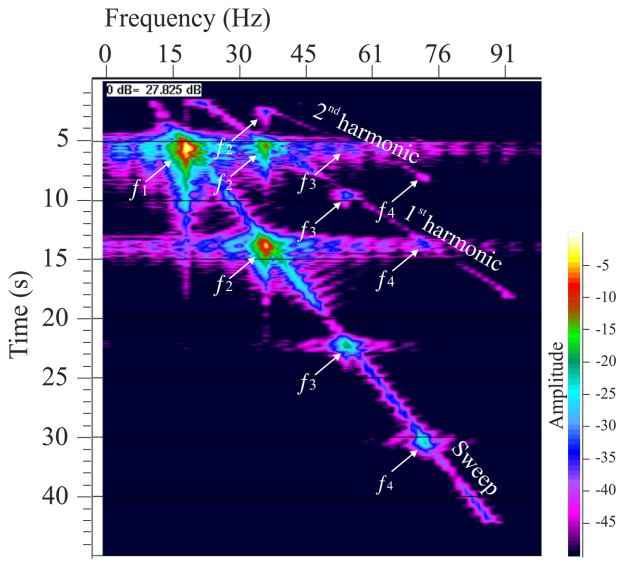

Figure 4 The FT amplitude spectrum, calculated for one raw uncorrelated strain seismic trace at 622.76 m MD, highlights frequency variations over time. A regular pattern of oval-shaped maxima can be observed at 18, 36, 54, 72 and 90 Hz. The fundamental labelled as f1 and overtone modes as f2–f4.

RINGING NOISE ANALYSIS

Methodological background

To better understand the ringing noise, we have performed the frequency–time (FT) spectrum analysis of a single seismic trace, recorded at 622.76 m MD. We picked the data before correlation from the interval affected by ringing noise, which we already identified by examining the plot with the amplitude spectrum in the previous chapter. FT representations transform original data from the time–space domain to the time–frequency domain by performing a series of fast Fourier transforms within moving time windows. Using this type of analysis, we can study frequency–energy variations over time.

The energy of a vibrator sweep and its harmonics at VP 10 in Groß Schönebeck can be clearly visualized (Fig. 4) with the method described above. Also, we see a repetitive pattern of horizontally elongated zones with a significant amplitude increase at frequencies 18, 36, 54, 72, 90 Hz etc., which are marked with white arrows.

These high-energy areas at given constant frequencies may correspond to the natural frequencies of the oscillating system. When the instantaneous frequency of the sweep signal or its harmonics coincides with the string's natural frequency, the condition for resonance is met, and the amplitude becomes strongest. Reflected waves from both ends of the vibrating cable interval will interfere with each other constructively or destructively at different points of the wire and create a standing wave, which represents an oscillation in time but does not actually move in space. Consequently, the resulting noise pattern can be interpreted as interference of two separate waves travelling opposite directions.

The harmonics of a system specify the frequency pattern of the standing waves. The lowest natural frequency is called fundamental, frequencies above it are known as overtones. The place where the waves are superimposed destructively, and which has no movement is called a node. On the contrary, the geometrical place where the waves are constructively superimposed, and the string has its maximum amplitude is called an antinode.

The freely hanging section of the cable can be approximated by a physical model of a string with fixed ends. In this case, the antinodes are located at its ends and the nodes are formed in-between. Figure 5(a) shows a string configuration for the first four harmonics. The fundamental harmonic contains one antinode in the middle of the string, the second harmonic will have two antinodes, the third three antinodes etc.

The harmonics (f) for the standing wave can be described via the formula:

$$f_n = \frac{nV}{2L}, \tag{1}$$

where V is the velocity of the medium, L is the length of the string, and n is an integer, harmonic number.

In case of standing waves formed on a string with free ends, there will be the same formula for harmonics. However, the position of the nodes and antinodes will be swapped.

For the fixed ends, there is a curious detail related to the phase of the strain at the left and right ends of the string for odd and even modes. In case of odd n, the motion of the string ends is out of phase, and for even n it is in-phase (Fig. 5a).

As could be noticed from Figure 4 at a specific moment in time, the resulting strain of the string represents a superposition of the different modes. The highest contribution belongs to the modes generated by sweep energy. We will refer to them as the main modes of the string. Resonances created by sweeps harmonics add complexity to the resulting string motion, but in principle do not change the main mode generated by the sweep.

The transition of the main mode from odd to even will change the phase of the one end of the string. The phase alteration to the opposite will happen only for one end, which means that the string ends' resulting phases will differ. This disproportion in phases will create the zigzag pattern after correlation with different up and down velocities. Thus, the

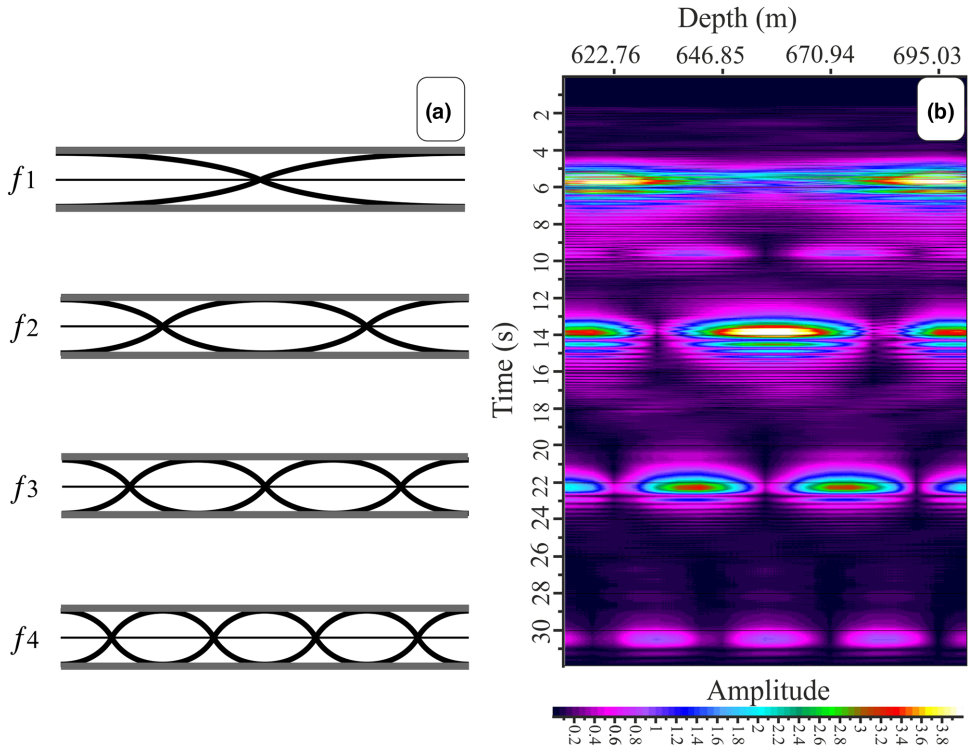

Figure 5 Standing wave modes for fixed-end cable vibrations for different frequencies. (a) Theoretical description of fundamental (f1) and overtone modes (f2–f4); the bold black line shows the cable strain for the corresponding frequency mode inside the borehole. (b) Reflection strength attribute calculated from raw strain data for the depth range from 611.26 to 701.30 m MD.

resulting dips of the noise on the correlated seismogram show phase velocities and depend on the standing wave frequency.

The reflection strength attribute (the modulus of the complex trace, or trace envelope) is calculated based on raw vertically stacked and uncorrelated distributed acoustic sensing (DAS) strain data for the depth region 611.26 to 701.30 m MD (Fig. 5b). This interval includes the seismic trace at 622.76 m MD, which we previously inspected in Figures 3 and 4. Hot coloured areas of the plot correspond to the antinode locations, black spaces between the loops show the position of the nodes in the current mode. The length of the vibrating cable interval can be estimated by visual inspection of the noise depth range, which in our example is approximately equal to 130 m. The fundamental mode (f_1) and three overtones (f_2, f_3, f_4) are clearly visible and have an identical configuration as the physical model (Fig. 5a).

Cable reverberation as a linear filter

Ringing noise has frequency characteristics similar to another unwanted phenomenon – ghost waves – occurring in marine seismic data. Backus (1959) described water reverberation mathematically as a linear filtering process. Strictly speaking in the case of the acoustically soft bottom (reflection coefficient $= -1$), the part of the equation corresponding to the ghost wave describing the water layer filter will accurately depict the standing waves formed inside the water medium.

Based on the equations described in Backus (1959), we could write a mathematical formula for the ringing noise frequency response function, with:

L: the length of the string = the length of the reverberating part of the cable,

V : the velocity of the acoustic wave travelling along the wireline cable,

R: reflection coefficient at the end of the string,

$\tau = 2\ L/V$: two-way travel time between two ends of the cable section,

n: integer index of reflection.

The resonance creates an impulse $\delta(t)$, which reverberates within a certain length of the cable. The resulting output at the receiver point $f(t)$ could be presented as bouncing reflections between two interfaces:

$$f(t) = \delta(t) - R\delta(t-\tau) + R^2\delta(t-2\tau) - \cdots, \quad (2)$$

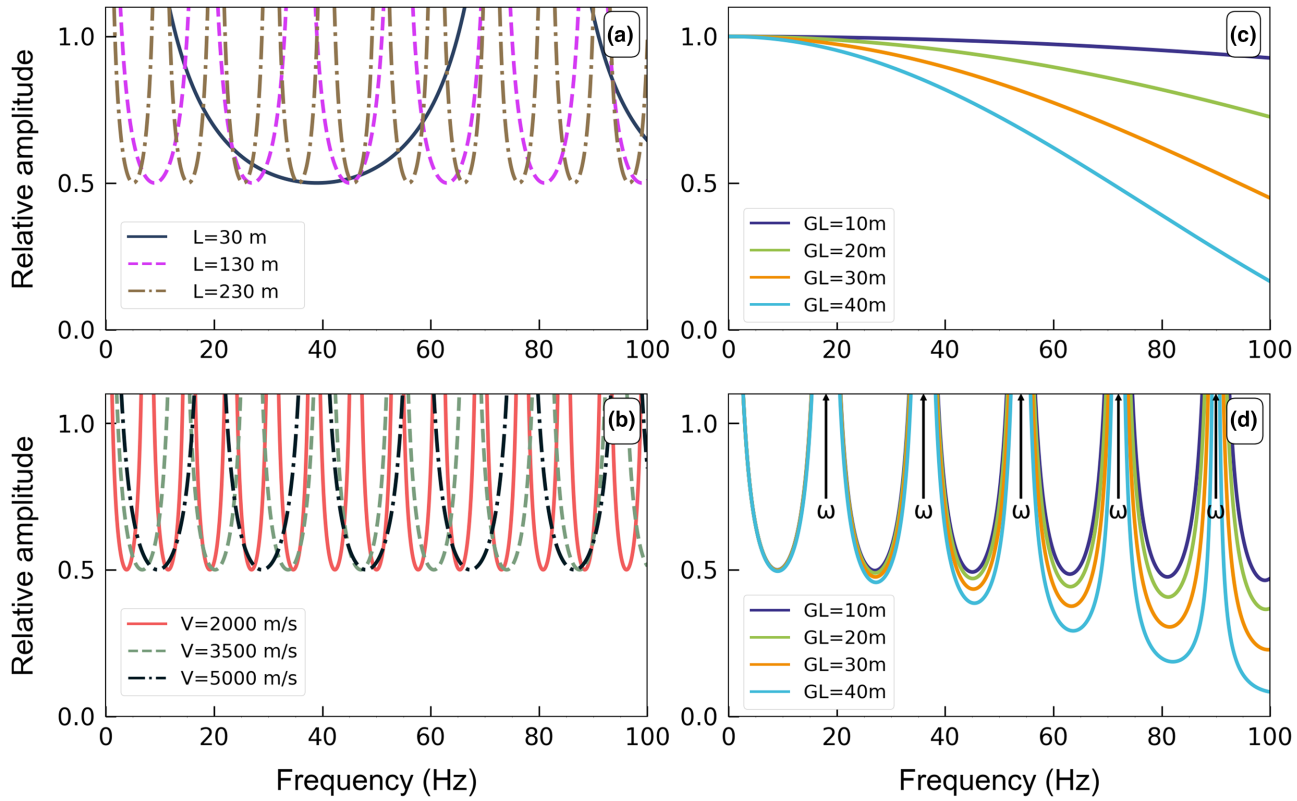

Figure 6 Effect of parameter variations on the ringing filter function (see text for the derivation of formula (9)). (a) Ringing noise frequency responses calculated for a string with different lengths (30, 130, 230 m; colour-coded). Wireline cable velocity is 4680 m/s. (b) Ringing noise frequency responses calculated for a string with different wireline cable velocities (2000, 3500, 5000 m/s; colour-coded). String length is 130 m. (c) Frequency responses for different gauge lengths (GL; colour-coded; velocity 4680 m/s). (d) Frequency response functions expected from the application of different gauge lengths (GL; colour-coded) to the ringing noise frequency response for a string length of 130 m and wireline cable velocity 4680 m/s; ω, resonating frequencies.

$$f(t) = \sum_{n=0}^{\infty} (-1)^n R^n \delta\,(t - n\tau)\,. \tag{3}$$

The frequency response $F(\omega)$ is represented as

$$F(\omega) = \int_{-\infty}^{\infty} \sum_{n=0}^{\infty} (-1)^n R^n \delta\,(t - n\tau)\exp(-j\omega t)\mathrm{d}t, \tag{4}$$

$$F(\omega) = \sum_{n=0}^{\infty} (-1)^n R^n \exp(-jn\omega\tau), \tag{5}$$

which is the binominal expansion for

$$F(\omega) = \frac{1}{1 + R\exp(-j\omega\tau)}, \tag{6}$$

$$|F(\omega)| = \left(1 + R^2 + 2R\cos(\omega\tau)\right)^{-1/2}. \tag{7}$$

The phase response $\phi(\omega)$ can be described by the following formula:

$$\phi(\omega) = \tan^{-1}\frac{R\sin(\omega\tau)}{1 + R\cos(\omega\tau)}. \tag{8}$$

In the case of $R = -1$, a condition is required for standing wave existence, and equation (7) will become

$$|F(\omega)|_{R=-1} = |1/2\csc(\omega\tau/2)| \tag{9}$$

with resonating frequencies described by formula (1). Thereby, the resulting formula (9) corresponds to the classical equation for standing waves harmonics in the case of both free and fixed ends.

Different effects of parameter variations on the ringing filter function of formula (9) can be analysed (Fig. 6). The decrease in length of the string leads to an increase of the first resonating frequency and overall stretching of the notch areas, as well as the resonating areas (Fig. 6a). The reduction of the

velocity values has the opposite effect: the smaller the velocity, the lower the fundamental frequency (Fig. 6b). It should be noticed that the wireline cable velocity (V) depends on the parameters string tension (T) and mass per length (μ) as follows:

$$V = \sqrt{T/\mu}. \tag{10}$$

Thus, a variation of the cable tension will change the cable velocity. Similar to the guitar tuning process, additional tension will create a higher frequency of the fundamental tone.

For DAS measurements, the gauge length parameter has a significant effect on the signal-to-noise ratio of the data as well as on resolution. Basically, it acts like a spatially averaging filter. Dean *et al.* (2017) describe the gauge length (GL) frequency response $Rgl(k)$ with wavenumber k by the formula:

$$Rgl\,(k) = \frac{\sin\,(\pi k GL)}{\pi k}. \tag{11}$$

Figure 6(c) shows frequency responses for four different gauge lengths calculated for a wireline cable velocity of 4680 m/s. It can be seen from the graph that for such a high velocity, we do not see any notches in the first 100 Hz. However, increasing of the GL value leads to decreasing of the first notch position, and the gauge length response function becomes steeper.

It is required to combine the frequency response of the ringing noise with the frequency response for the gauge length to estimate the influence of the ringing noise filter on the DAS data. The resulting filter frequency response function (Fig. 6d) evidences that an increase of the gauge length leads to stronger attenuation of higher frequencies. In the example given, the effect causes a decrease of the amplitude response from 0.5 (gauge length 10 m) to 0.1 (gauge length 40 m). This is important to note because such an effect will also smear out the noise.

Ringing noise filter tests

To illustrate the impact of the ringing noise filter, we performed simple modelling using the raw pilot sweep from the start-up tests (10–88 Hz, linear, 36 s length), which we had used for data acquisition and correlation (Fig. 7). The spectrum of the sweep has a rectangular shape with tapered ends. Using formula (9), we modelled the ringing noise response function. Notice that it has a series of narrow areas where the amplitude is approaching infinity (around 18, 36, 54 Hz etc.) alternating with notches, existing in the original spectrum (around 27, 45, 63 Hz etc.). The application of the ringing noise filter causes disturbances at the sweep spectrum and creates a series of peaks and troughs in the spectra. Additional application of the gauge length frequency response will lead to loss of energy at frequencies higher than 80 Hz. A similar amplitude spectrum behaviour we observe in the data.

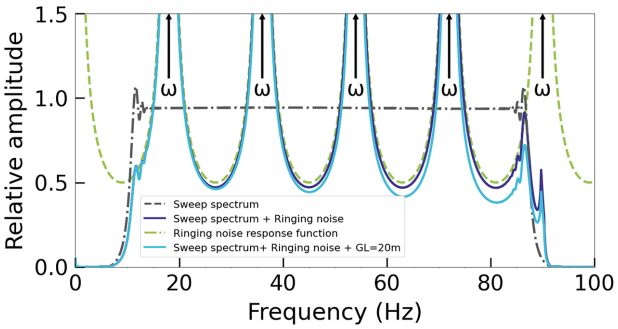

Figure 7 Comparison of an original sweep spectrum and colour-coded the spectra after different filter applications (parameters used: wireline cable velocity 4680 m/s; string length 130 m; gauge length 20 m).

NOISE ELIMINATION WITH KNOWN PROCESSING METHODS

Cable reverberations create a sequence of distinct peaks and notches in the frequency spectrum. This decreases the useable bandwidth of the measured wavefield and, as a result, reduces the vertical resolution of the data. The existing processing methods for ringing noise elimination can be classified into three main categories: wavefield extraction methods, statistical methods and subtraction of modelled noise. We briefly summarize the first two approaches here, being accompanied by the application to the Groß Schönebeck distributed acoustic sensing VSP data.

Wavefield extraction methods

Wavefield extraction methods attempt to reconstruct the wavefield using information from neighbouring traces and then substitute the noise. According to the Fresnel zone theory, noisy traces should have similar characteristics as unaffected neighbour traces. We have used the time–frequency domain (TFD) filtering method (Elboth *et al.*, 2008) that replaces anomalous amplitude values with an amplitude estimated from adjacent traces. Using a short Fourier transform algorithm, a median magnitude of each trace's spectrum is calculated within a specified filter length and frequency subband.

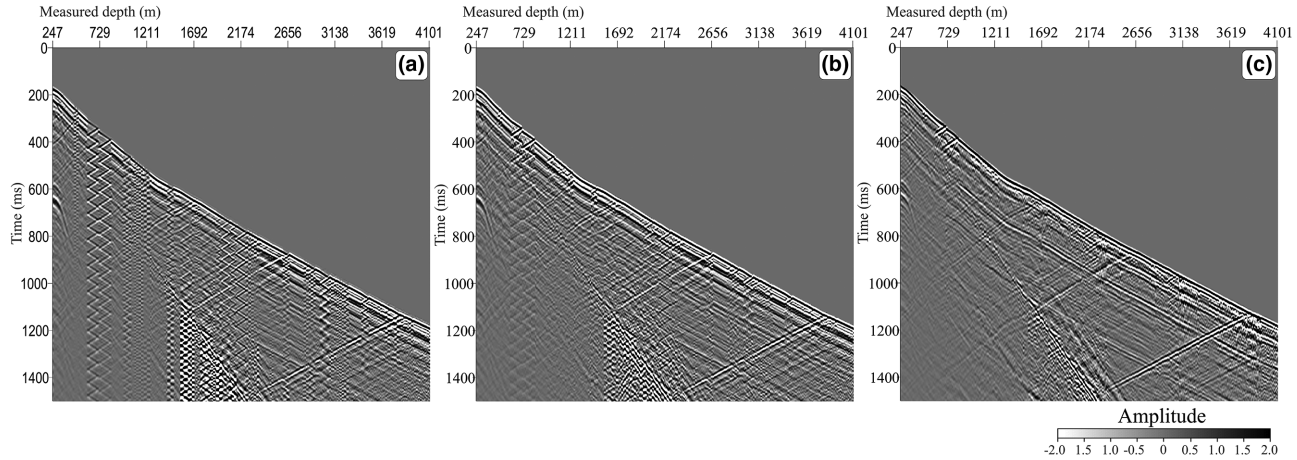

Figure 8 Comparison of measured and filtered common source gather: (a) before denoising, (b) after time–frequency domain noise attenuation and (c) after Burg adaptive deconvolution.

On the source gather before denoising (Fig. 8a), there are many depth intervals with poor coupling. Application of the TFD to the Groß Schönebeck data shows its potential to significantly reduce the amount of ringing noise in the data (Fig. 8b). We can see a particular reduction of the ringing noise at 1200–1933 m depth interval. Nevertheless, when the spectral amplitude values are similar, the algorithm will be unable to clean the data completely. The residual noise can be seen in Figure 8(b) at 488–970 m, 1933–2174 m and 2897–3138 m depth ranges. This is the main drawback of this method.

Statistical methods

Statistical noise estimation relies on spectrum balancing and adaptive filter construction without previous knowledge about the noise. We have evaluated several deconvolution algorithms for computing prediction error filters like Wiener-Levinson, L1 or L2 Norm and Burg's maximum entropy approach. Standard spiking or predictive deconvolution is robust under a wide variety of input conditions. However, a substantial improvement in pulse compression could be obtained by the Burg algorithm (Burg, 1972; Burg, 1975) in an adaptive formulation (Griffiths, Smolka and Trembly, 1977; Hale, Widrow and Stearns, 1985) for our type of data consisting of non-minimum phase wavelets combined with sparse reflectivity series. This method relies on the assumption that the power spectrum is an output of the hypothetical linear system, which has generated the signal. That, in turn, leads to an improved spectral estimation and minimized end-effect problems if a moderate adaption rate is chosen.

The deconvolution has a dual effect on the data: it suppresses monofrequent noise and whitens the amplitude spectrum. By the use of the Burg adaptive deconvolution to the Groß Schönebeck data, the signal of the seismic traces is clearly sharpened. The application of the Burg method (Fig. 8c) allowed cleaning the data from the ringing noise almost completely, with small residuals around the first-break arrivals at the following depth intervals: 604–861 m, 2121–2270 m, 2969–3138 m. As a result, we were able to improve resolution and reflection continuity.

MATCHING PURSUIT DECOMPOSITION WITH GABOR ATOMS

Supplementing the application of the two known methods given above, we introduce here a new approach we termed matching pursuit decomposition (MPD). It belongs to the category of physical modelling of the noise and its subsequent subtraction from the data. Cases described in the literature mainly differ in their approach for noise modelling (e.g. Yu *et al.*, 2016a).

The problem of signal and noise wave separation is always relevant in a seismic data processing flow. Standard approaches use frequency and velocity filters to eliminate unwanted components from the seismic data. These filters work without considering the spatial–temporal position of the noise, and they do not allow to identify the signal patterns. In response to this problem, various time–frequency decomposition techniques were developed, for instance, decomposition of a signal with redundant dictionaries consisting out of Gabor functions. Signal decomposition methods allow splitting

the wavefield into waveforms, characterizing their frequency, amplitude and duration of oscillations in time (cf. Mallat and Zhang, 1993). These algorithms are applied in various areas, including noise reduction and filtering (Wawrzyniak, 2006; Ozbek, Özdemir and Vassallo, 2008; Wang, 2010; Ahmed, 2012; Chen, Li and Cheng, 2018). Nevertheless, there are only a few examples of signal decomposition with redundant dictionary techniques applied to the ringing noise problem.

Unlike previous works on the ringing noise problem (Yu *et al*., 2016a; Chen *et al*., 2019), we advocate here (1) applying atomic trace decomposition on raw strain data, (2) modelling of the ringing noise with an overcomplete Gabor atoms dictionary and, finally, (3) subtracting it from the signal. The hypothesis to test is whether localization and elimination of the noise before correlation prevents the smearing of the noise by the correlation process and therefore leads to better denoising and thus imaging results.

The matching pursuit (MP) algorithm is the successor of the class of algorithms called 'atomic decomposition'. We have used the MP code from the MP5 and Svarog projects (Kuś, Różański and Durka, 2013; The Svarog developers team, 2014; Durka *et al*., 2015; The Svarog developers team, 2016). The code is distributed under the GNU General Public License v3.0.

The MP algorithm has four main steps:

1. Set the initial signal as a current residual of the decomposition.

2. Select the basic function (atom) which provides the maximum magnitude of the scalar product of the selected atom and the current residual of the signal. The selection process also includes the mechanism of the local readjustment to the local properties of the signal.

3. Calculate the new residual of the signal by subtracting the selected atom from the current residual.

4. Check the stop condition of the signal decomposition.

In the implemented algorithm, there are two scenarios of how the computation can stop. First, if the desired accuracy of the signal approximation is achieved, i.e. when the subselected atoms explain the pre-set percent of the signal's energy, the calculation stops. A second stop criterion is based on a reasonable runtime, implemented as a check for the maximum number of iterations, i.e. if the specified number of iterations is exceeded, then the decomposition process emergently stops. Usually, the valid number of iterations is determined experimentally for a particular type of signal and specific dictionary.

The reconstruction result of the original seismic trace is a linear combination of waveforms (atoms). The result of the processing is an ordered list of basic functions called 'atoms'. It starts from the atoms with the highest magnitude, with the highest influence, and goes down to the signal's weakest parts. They are characterized by specific parameters (modulus, amplitude, position, scale, frequency, phase), which represent time–frequency properties of the corresponding waves.

The quality of decomposition was evaluated using the formula for cross-correlation (*CC*) between the original seismic trace and the reconstructed trace (Semnani *et al*., 2019):

$$CC = \frac{\sum_{n=1}^{N} \left(f(n) - \mu_f\right)\left(\hat{f}(n) - \mu_{\hat{f}}\right)}{\sqrt{\sum_{n=1}^{N} \left(f(n) - \mu_f\right)^2} \sqrt{\sum_{n=1}^{N} \left(\hat{f}(n) - \mu_{\hat{f}}\right)^2}} \times 100\%, \tag{12}$$

where $f(n)$ is the original signal, $\hat{f}(n)$ denotes the reconstructed signal, μ_f and $\mu_{\hat{f}}$ represent the mean values of $f(n)$ and $\hat{f}(n)$ respectively, and N is the number of signal samples.

The main property of MP algorithms is the suboptimal selection of basic functions (atoms) from the dictionary. This property allows to run the algorithm and to get the result in an acceptable time. Such algorithms are called 'greedy'. At each step (iteration), only local optimization is performed. It is assumed that the final result will be optimal for specific practical goals. Suboptimal algorithms are applied in practice when there are no exact and efficient algorithms, or the existing algorithm has such complexity that, in general, a solution to a problem cannot be obtained in acceptable computation time.

The key advantages of this decomposition are the ability to perform a sparse representation of data and adapt to a specific signal. Nonlinear methods help find the optimal representation for a particular signal on the redundant set (called a dictionary) of the basic functions. The overall procedure is somewhat similar to the visual examination of the signal.

Decomposition results for the Groß Schönebeck data

We calculated the MPD of the whole vertical seismic profiling section for VP 10 from the Groß Schönebeck data set. For SEG-Y file reading we used the ObsPy 1.1.0 python library (Krischer *et al*., 2015; The ObsPy Development Team, 2017).

The process of ringing noise model construction could be described as follows:

1. Decomposition of each original distributed acoustic sensing (DAS) seismic trace to 80 atoms with pre-set 95% recovery of the original signal. A table with parameters (modulus, amplitude, position, scale, frequency, phase) for each atom is written to a separate csv file.

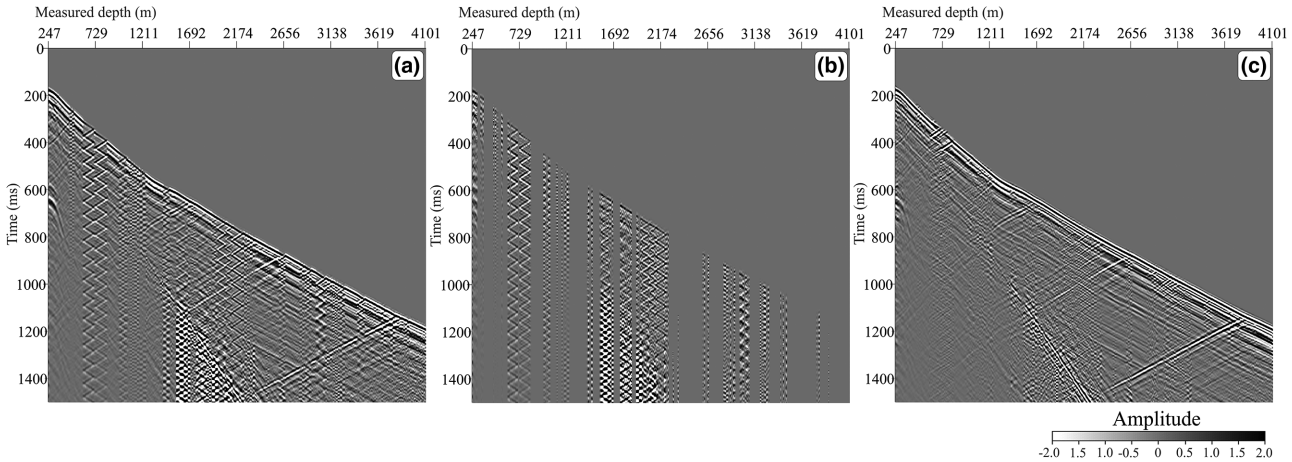

Figure 9 Comparison of measured and processed common source gather: (a) before denoising (same as in Fig. 8a); (b) MPD noise model; (c) after noise model subtraction.

2. Checking the current trace for the resonance conditions (anomalous amplitude values in the recorded seismic trace):

a. Determining a threshold value for the trace selection process. The threshold value is determined as a product of the mean value of the standard deviations for amplitude values of the original DAS trace in 500 milliseconds moving window and a multiplier.

b. Compare the standard deviation for amplitude values of the current atom calculated in 500 ms moving window with the threshold value estimated during step a.

- If the standard deviation of the current atom exceeds the threshold, then this trace will be used to define atoms selection for the noise model.
- Otherwise, the trace is marked as 'clean' and further analysis is not required.

3. Calculate kernel density estimation (KDE) for frequency values of atoms (Waskom *et al.*, 2017).

4. Find peak on KDE. A search of the peaks could be regulated through adjusting the prominence parameter.

5. Select all atoms which have frequency parameters falling into the interval (peak frequency −2.5 Hz, peak frequency +2.5 Hz).

Computations are performed for each trace independently, and hence, computations could be easily performed parallelly, increasing the total processing speed.

After analysing the original seismic DAS traces and the atoms of decomposition results, we generated a model of the ringing noise, which we could use for data denoising (Fig. 9). Compared with the original data (Fig. 9a; with standard preprocessing consisting of vertical stacking, correlation with the pilot sweep and subsequent differentiation applied), we observe that amplitude and phase of the modelled ringing noise (Fig. 9b) accurately reconstruct the noise. The created noise model was subtracted from the original raw strain data, and the same preprocessing flow was applied to the seismic section (Fig. 9c). A closer zoom clearly shows an improvement of the seismic section after denoising (Fig. 10). Noise has been mostly eliminated (Fig. 10b, d, f and h). Nevertheless, in some parts of the data, we see small residuals. At a depth interval around 719 m (Fig. 10b), the first-break arrival was already significantly corrupted, and the noise model was unable to correct for this effect. In some cases, the noise model does not include ringing signals with a lower amplitude due to the threshold parameter so that it leads to a low-amplitude residual, for instance around depth 3138 m (Fig. 10f).

At the depth level of 1200 m, there is a DAS strain trace, which contains a high amount of the studied high-frequent noise (Fig. 11a). After subtraction of the noise model (Fig. 11b), the main part of the ringing noise was eliminated. The overall shape of the cleaned DAS seismic trace revealed different characteristics (Fig. 11c). The areas where we see the change of the seismic trace character are located at those places where we had the maximums on the ringing noise model. For instance, between 5 and 10 s and 15 and 20 s, we see a lowering of the amplitude values and a change of the envelope of the seismic signal. The highest amplitude occurs now at 16.122 s and is 0.33, which is 3.3 times lower than the highest amplitude of the original trace. Thereby, the processed DAS trace also becomes more similar to the accelerometer trace (Fig. 11d).

This amplitude and waveform behaviour can be further analysed by calculating FT spectra (Fig. 12). The propagation

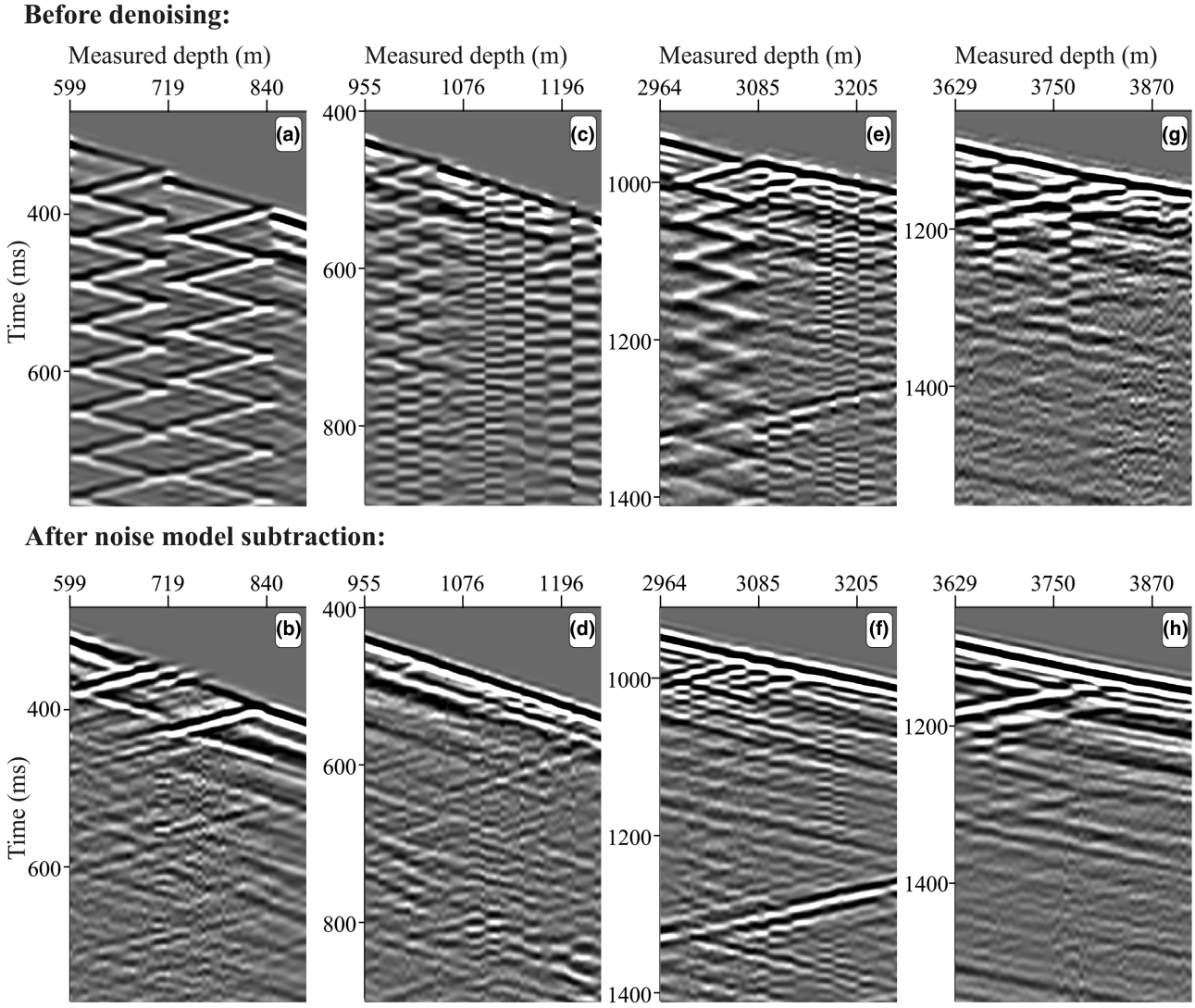

Figure 10 Zoom of the seismic sections shown in Figure 9(a and c). Four upper panels (a, c, e, g) show four different parts of the seismic section after preprocessing, and the four lower panels (b, d, f, h) after additional MPD denoising.

of the sweep energy from 10 Hz up to 88 Hz at the depth level of 1200 m MD is clearly recognizable in the unprocessed DAS trace (Fig. 12a), containing strong disturbing signals that are revealed by ringing noise modelling (Fig. 12b). Around 45 Hz, there are distinct oval-shaped, smeared high-amplitude areas appearing at 2.3, 4.3, 7.7 and 18 s. These are resonances that were reproduced accurately. After denoising, the strong amplitudes at 45 Hz were significantly lowered down in the resulting DAS trace (Fig. 12c). Now we see the contributions from other frequencies to the signal more prominently, even a much smaller resonance at approximately 90 Hz. These peaks do not appear in our noise model, but they lie outside of the sweep range and will be filtered out by the correlation process. The strong continuous energy band around 45 Hz corresponds to the natural frequency of the vibrating cable interval. In other words, this is a frequency at which this part of the cable tends to oscillate without the influence of an external force.

In order to get a better understanding of our denoising results, we inspected amplitude-frequency spectra of the same DAS trace after preprocessing and compared it with reference measurements. The DAS trace spectrum before noise suppression has a distinct resonance peak at around 45 Hz (Fig. 13a). The selected Gabor atoms for the ringing noise model accurately mimic the shape of this peak. Consequently, the DAS spectrum after denoising process follows the shape of the original spectrum, except for the narrow range around

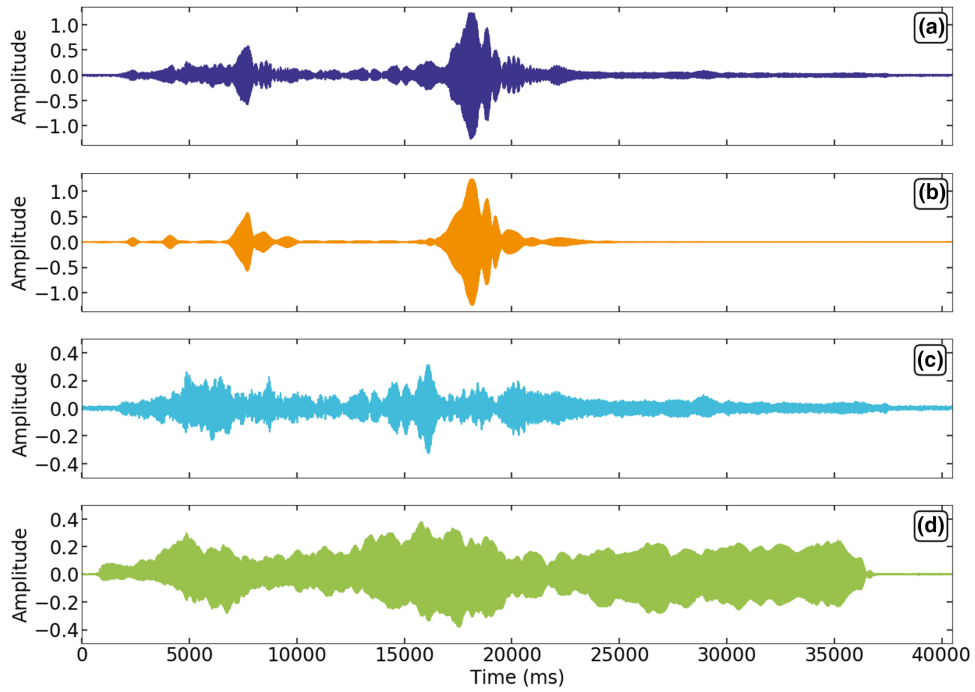

Figure 11 Comparison of measured and denoised DAS strain traces (depth level: 1200 m MD): (a) uncorrelated original trace, (b) modelled ringing noise, (c) trace after noise subtraction and (d) corresponding accelerometer point tool trace.

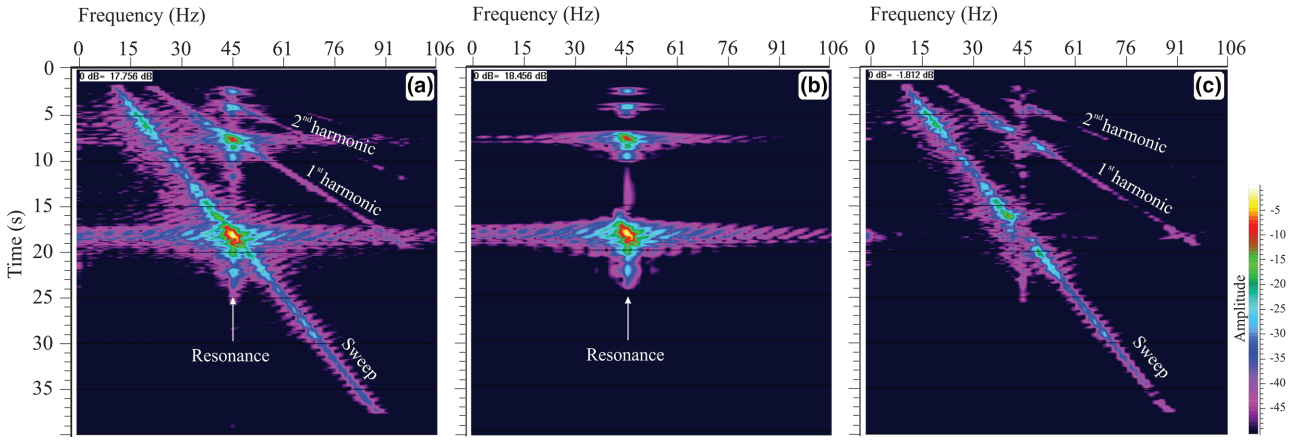

Figure 12 FT spectrum comparisons of DAS strain trace before and after noise subtraction (depth level: 1200 m MD). FT spectrum of (a) raw trace, (b) MPD noise model and (c) trace after noise model subtraction.

the resonating frequency, which influence was lowered down. It should be noticed that the spectrum of the VSI tool measurements has greater levels for higher frequencies in comparison with the DAS trace spectrum, most likely due to the filtering effect of the GL frequency response. In the time domain (Fig. 13b), we can also observe a significant improvement in terms of ringing noise elimination. The original DAS trace at 1200 m is strongly affected by ringing noise. After the first-break arrival around 520 ms, we only see a sinusoidal noise pattern, but after ringing noise subtraction the DAS trace starts to resemble the VSI trace.

CABLE COUPLING IMPROVEMENT METHODS

Processing-based solutions are always limited by quality of the initially recorded data. A certain percentage of the energy emitted by vibrators is converted into standing waves on the wireline cable, which reduces the S/N ratio. By reducing

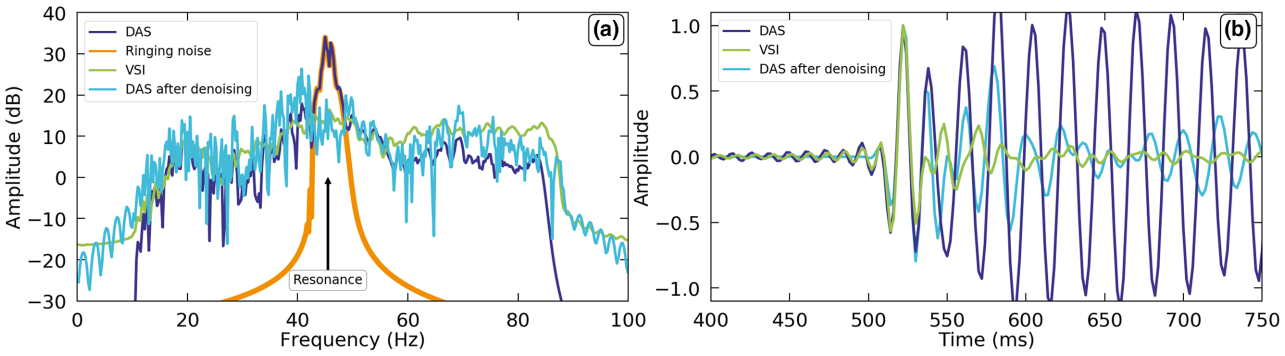

Figure 13 Comparison of DAS and accelerometer point tool traces (VSI). The preprocessing applied to all data sets comprised vertical stacking, correlation with the pilot sweep and subsequent differentiation; depth level is 1200 m MD. (a) Amplitude spectrum for DAS trace before denoising (moderate dark blue solid curve), for DAS trace after ringing noise model subtraction (light blue solid curve), for ringing noise model (solid orange curve) and accelerometer point tool (light green solid curve). (b) Comparison of a 350 ms fragment of the DAS trace before and after denoising with accelerometer point tool measurements (same colour-coding as in a).

vibrations of the cable, either the problem of the ringing noise could be avoided completely or the influence of it on the data can be significantly reduced.

Noise caused by cable reverberations is common in engineering (e.g. reverberations of power lines caused by wind) and geoscience (e.g. vortex noise due to marine cable towing behind the vessel) communities. In marine seismics, the problem is settled by the usage of cable fairings (Every, King and Weaver, 1982; Niedzwecki and Fang, 2013) that reduce water strumming and improve the quality of data acquisition. Munn *et al.* (2017) have demonstrated an enhancement of data quality in borehole surveys through an improved cable coupling. It was achieved by the application of a flexible liner, which presses the cable against the borehole wall. This installation is limited mainly to shallow boreholes with depths of 425 m or less. Constantinou *et al.* (2016) and Schilke *et al.* (2016, 2017) have described the idea that by adding slack to the wireline cable, one could create a twisting of the cable, and as a result, improve the coupling and decrease the noise amount in the data.

During the first day of acquisition in Groß Schönebeck, we conducted several start-up tests, which also included a slack test (Henninges *et al.*, 2021). We have collected four data sets for E GrSk 3/90 with 1, 5, 11 and 20 m slack applied to the cable. The data acquisition was performed with a 36 s long linear sweep 10–88 Hz and ten sweep repetitions. Figure 14 shows a comparison of these four data sets with some preprocessing applied (diversity stack, correlation with the pilot sweep, time differentiation).

We cannot observe significant changes in the ringing noise distribution, although there is a certain improvement, for example at 1878–2384 m depth between the 5 m and 11 m slack tests data sets (see Fig. 14b and c). After increasing the slack due to cable redistribution, the coupling in this area was probably improved. Nevertheless, the data set with 20 m slack shows some ringing again in the same depth range (cf. Fig. 14d). The ringing noise between 2760 and 3016 m shows similar behaviour. However, the noise zone at approximately 2890 m MD is significantly decreased when 20 m cable slack was applied (Fig. 14d), in comparison with the recording of the same depth interval using 1, 5 and 11 m slack (Fig. 14a–c).

After increasing the slack, we have also noticed a dropping of the amplitude level from first arrivals close to the zone with reduced ringing signals (cf. Henninges *et al.*, 2021) and Zechstein bottom reflections (see Fig. 14, green arrows) in the deeper part of the seismic section. Since the experiment was focused mainly on depths greater than 3700 m, we tuned the best possible cable performance for this range. Therefore, after analysing the start-up test results, we continued the experiment with almost full tension applied to the cable.

DISCUSSION

Comparison of processing-based methods

During the past years, there has been considerable interest in finding the appropriate approach to decrease ringing noise in wireline distributed acoustic sensing (DAS) data and clean the spectrum. A technical solution which will allow achieving a better cable coupling during the data acquisition is preferable. However, the improvement of the cable coupling during wireline acquisition remains a nontrivial process. Moreover, the results of the slack tests conducted at Groß Schönebeck

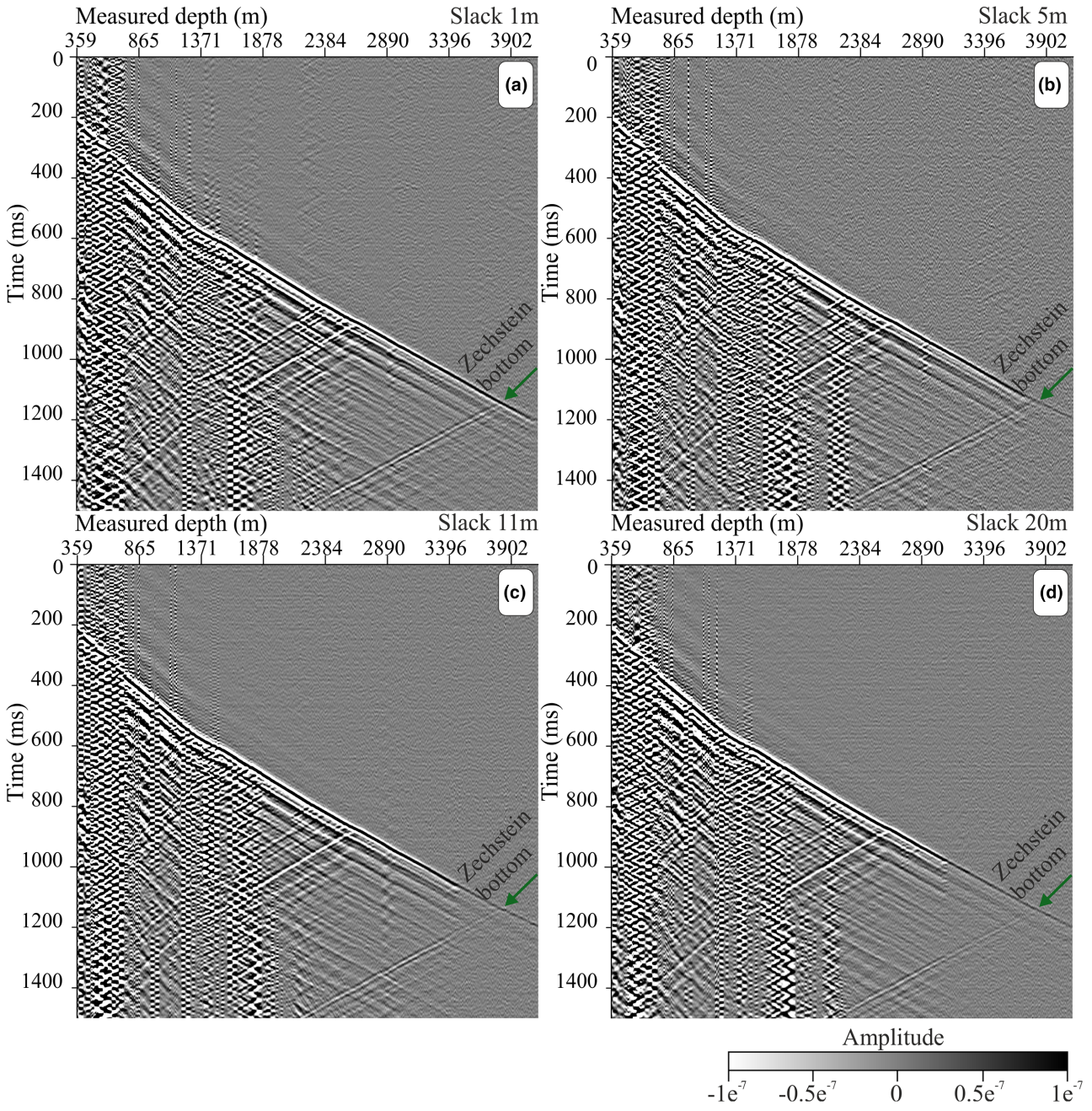

Figure 14 Comparison of common source gathers recorded for VP10 in E GrSk 3/90 well and acquired with different cable slacks: (a) 1 m, (b) 5 m, (c) 11 m and (d) 20 m slack. Green arrows on seismograms annotate position of Zechstein salt bottom reflection.

showed that the suggested modifications of the current acquisition techniques such as lowering of extra cable to the borehole can lead to a decrease of the noise and the reflection signals. The observed reduction of the S/N ratio in the region of cable accumulation is consistent with the results of the experiment described by Constantinou *et al.* (2016) for the data set acquired at Rittershoffen, France, and should be further investigated. Therefore, taking into account the mentioned technical limitations, in the present study, we concentrate on the processing-based solutions and demonstrate several ways of tackling the ringing noise problem for the data acquired at the Groß Schönebeck geothermal site.

The comparison of the methods used for data denoising in this study is shown in Figure 15. A significant part

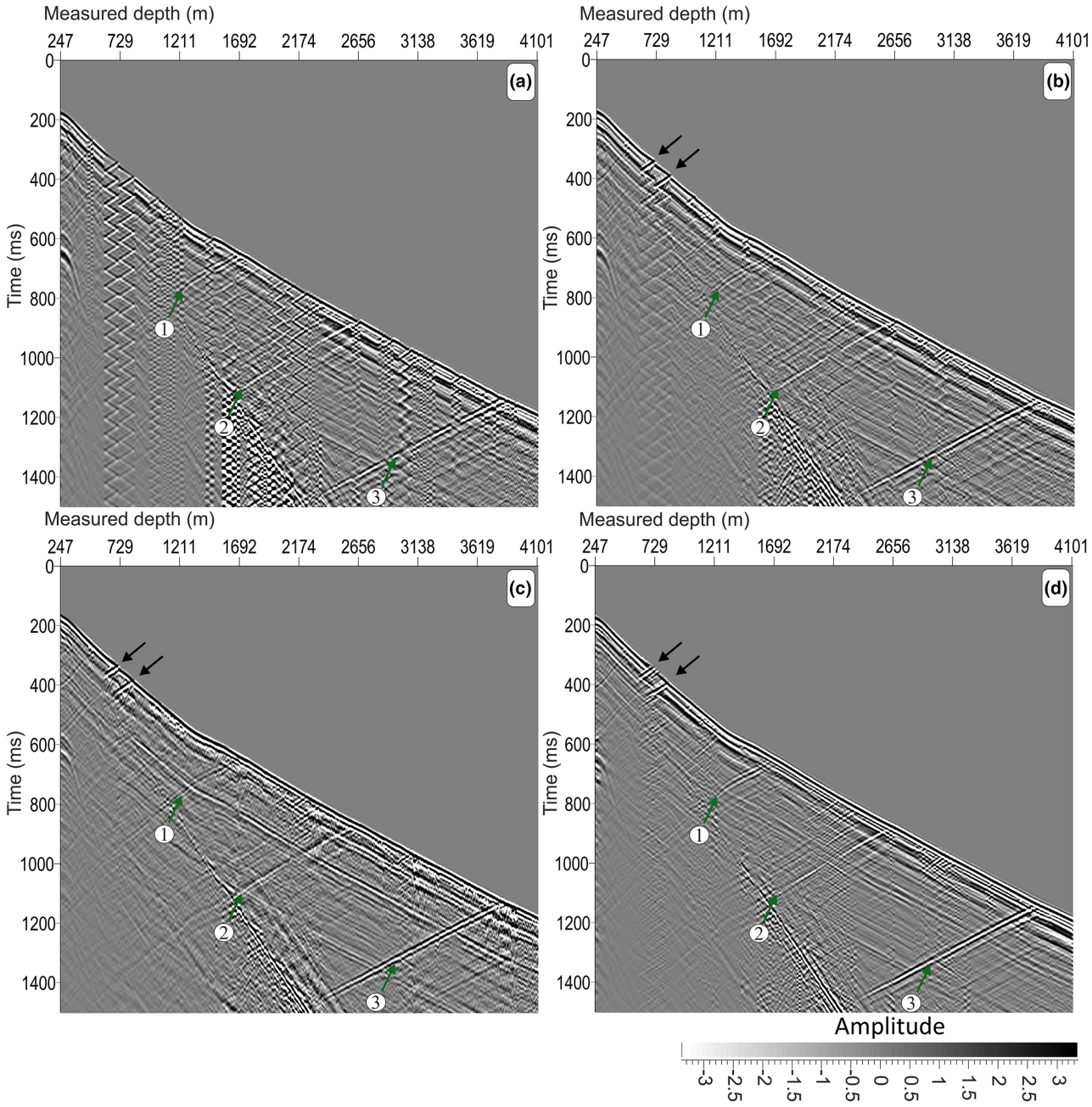

Figure 15 Comparison of the effect of different processing methods applied for ringing noise elimination. Common source gathers (a) before denoising, (b) after time–frequency domain noise attenuation, (c) after Burg adaptive deconvolution, d) after noise subtraction based on signal decomposition with Gabor atoms. Applied preprocessing consisted of vertical stacking, correlation with the pilot sweep and subsequent differentiation. Moderate coherency enhancement was additionally applied post-processing with methods b, c and d. In all panels, green arrows indicate reflections at different depth levels. In all panels, green arrows with numbers on seismograms mark positions of the main reflectors at different depth levels: 1, Buntsandstein; 2, Zechstein top; 3, Zechstein bottom. Black arrows mark example of depth levels with residual ringing noise.

of the observed noise (for example, at depth interval 1211–2656 m in Fig. 15a) is suppressed after TFD noise rejection (Fig. 15b). Similar noise reduction results are obtained by applying the Burg adaptive deconvolution, seen in Figure 15(c). Finally, yet importantly, our newly shaped and denoising method based on matching pursuit decomposition (MPD) with Gabor atoms clearly outperforms previous denoising results (Fig. 15d). However, there are certain differences and limitations for the application of the techniques that we discuss here.

The *TFD noise rejection* is a well-known standard processing instrument, which is available in many professional software packages (e.g. Promax (Halliburton), Omega (Schlumberger), Geovation (CGG)). It is used for elimination of various noise types of different nature in seismic data such as ground roll, swell noise, wind noise etc. The process will improve a seismic record successfully, as long as the noise and the signal have different amplitude and frequency characteristics. In the case of similar characteristics, a reduction of the filter amplitude threshold will lead to noise elimination and to signal degradation at the same time. The application of the TFD is a more advanced way of data filtering in comparison with a median filter approach used by Bakku *et al*. (2014) for gas exploration and a simple notch filter applied in Miller *et al*. (2012) at the Devine test site in an active oil and gas province. In practice, accurately tuned frequency sub-bands selection criterion in TFD allows performing more accurate filtering in the frequency band of the data. Moreover, the use of the information from the adjacent traces makes the process of the ringing noise elimination more robust and minimizes the waveform distortion after filtration. Altogether, the TFD method gives a quick and reasonable result with relatively low computational cost.

For the Groß Schönebeck data, TFD noise rejection allowed to suppress quite a substantial part of the ringing noise. There are different depth levels with good (see 1211–1692 m; Fig. 15b) and reasonable noise suppression (for instance, 1933–2656 m; Fig. 15b). Although the signal-to-noise ratio of the seismic section after TFD processing has been improved, there are however still some areas with residual noise with decreased amplitude (for example 2897–3379 m depth interval in Fig. 15b) and one interval with particularly high noise residuals and distorted first-break arrivals (see black arrows in Fig. 15b).

The application of the *Burg adaptive deconvolution* is also a quick and efficient tool for the ringing noise problem. This powerful spectral balancer has several advantages: good results can be achieved even with a general mixed-phase wavelet if the beginning of the wavelet rises sharply and the reflection coefficients are not assumed to be quite randomly distributed. The adaptive approach also takes account of wavelets that are varying with time. The main drawback of the technique is its sensitivity to high-frequency noise, which will be often amplified. Therefore, careful amplitude balancing of the data is required before application of the Burg adaptive deconvolution approach.

Most recently, Willis *et al*. (2020) have developed another statistical approach for ringing noise elimination based on the analysis of the noise periodicity and gap deconvolution. The identification of the ringing noise period is based on the identification of the X-like pattern on adjacent autocorrelated traces. The main difference with Burg adaptive deconvolution is that adaptive operators are replaced by prediction and adaptive subtraction. Burg adaptive deconvolution performs general equalization of the spectrum. It works without any prior information, while the application of the gap deconvolution in the approach of Willis *et al*. (2020) requires the knowledge of the noise period. If evaluated prediction distance is not accurate, this can lead to errors in ringing noise multiple reflections, yielding distortions and leaving the residual noise energy behind. However, since both cable reverberation inside the borehole and ghost wave generation in marine seismics represent a standing wave phenomenon, the application of classical deghosting filters for source ghost elimination (Song, Gong and Li, 2015; Wang *et al*., 2015) would also be a valid option for DAS data denoising. The proposed method for the ringing noise period evaluation by Willis *et al*. (2020) can be used for calculations of the deghosting filters.

After application of the Burg method to the Groß-Schönebeck data, almost all ringing noise is omitted with small exceptions at some depth levels (for example, see black arrows in Fig. 15c). Nonetheless, the Burg result has some signal distortions associated with deconvolution in the areas of ringing noise residuals, for instance, at 2318 and 3138 m depth. In general, adaptive deconvolution considerably improved the denoising results in comparison with the TFD method here.

As a new approach, we calculated a noise model based on the results of *MPD with Gabor atoms* and subtracted it to clean the DAS data (Fig. 15d). The method of trace decomposition allows in principle to separate the noise and the signal, even for the case when they are overlapping both in time and frequency domains. Thus, this processing technique is a powerful tool, which in combination with the physical understanding behind the noise generation process, allows to perform a sophisticated data analysis and significantly improve signal quality. However, the average computation time is

estimated approximately three times higher than for TFD and Burg adaptive deconvolution.

The application of MPD for coupling noise elimination can be attributed to the group of methods which attempt to use different ways of modelling for denoising purposes. The first work in this direction was published by Yu *et al.* (2016a). Although the authors have demonstrated the successful application of their method on the real field data, the proposed DAS coupling noise suppression requires the estimation of the noise attenuation characteristics, which might be challenging.

Algorithms based on sparse optimization decomposition can handle uncertainties such as amplitude fitting and consider changes of the coupling noise characteristics between the different zones of the well where the cable exhibits oscillation motion. Such decomposition method has been employed by Chen *et al.* (2019). Based on the morphological analysis of the DAS data characteristics, the authors propose using the continuous wavelet transform and the discrete cosine transform as the sparse dictionaries to represent signal and coupling noise, respectively. Arriving from a synthetic example to field data, Chen *et al.* (2019) emphasize that decomposition of the complex seismic response is a nontrivial process and requires a combination of the overcomplete dictionaries. To simplify this step, in our work, we came up with an idea of applying a single overcomplete dictionary based on the Gabor basic functions (atoms). The proposed dictionary is commonly used for seismic waveform representations and is easy to handle. Tests performed on the Groß Schönebeck field data demonstrate promising results. However, the application of overcomplete types of dictionaries should be further investigated in the future.

The use of MPD improves ringing noise detection and suppression and therefore increases the overall reflection coherency in the data. Thus, MPD with Gabor atoms has the best potential in terms of applicability for ringing noise elimination in wireline DAS data. The visual interpretability of the seismic reflections, marked by green arrows in Figure 15, increases gradually from Figure 15(a to d). Nevertheless, there are also some noise residuals after MPD at the similar depth regions as in the Burg adaptive deconvolution result (Fig. 15c and d; black arrows). The distortion of the initially recorded strain data in these parts of the seismic record was already quite significant. Therefore, MPD, as well as Burg's method, is not able to restore it. Overall, accurate data analysis and the application of the proper denoising method allowed to increase data quality significantly. As a result, the corridor stacks (Henninges *et al.*, 2021) and the vertical seismic profiling imaging results at the Groß Schönebeck site were improved.

Effect of velocity on data acquisition

Overall, after analysis of our denoising test results, we can conclude that there is still a valid signal below the noise but depending on the number of peaks and notches (cf. Fig. 6), the useful part of the signal might also be decreased. The efficiency of the coupling noise removal from the data depends on difference between noise and signal characteristics, in particular on the velocity values for fibre optic cables and velocity of the formation. The estimation of the standing wave velocity can be easily derived from equation (1):

$$V = \frac{f_n 2L}{n} \tag{13}$$

where n is the integer harmonic number, f_n is the the frequency of the nth harmonic, L is the length of the theoretical string, which is equal to the length of the noisy interval in the data. However, we must keep in mind that this simple calculation can be used only for velocity estimation because it does not account for the cable tension. Also, the gauge length smears up the zone of the noise.

An average velocity of the noise for the presented data set is approximately equal 4400 m/s, which is close to values typical for fibre optic cables (ca. 5000 m/s; Raisutis *et al.*, 2016). Chang and Nakata (2020) report similar values of the noise velocities at the Brady geothermal field.

In the Groß Schönebeck case, the local reservoir rock led to very uniform reflection dips for both the ringing noise and the seismic reflections. Consequently, the denoising method is sometimes not able to suppress ringing noise entirely in case of reflections with similar slope lying under the noise; this prevents the algorithm from distinguishing between noise and signal. Therefore, a possible overlap of reflection and ringing noise should already be considered during planning and interpretation.

CONCLUSION

Wireline distributed acoustic sensing still has limitations during field measurements that cannot entirely be overcome by subsequent processing. However, since fibre optic methods develop rapidly, the problem of coupling noise should be further tackled also during the development of field acquisition tools.

The presented new denoising method based on a matching pursuit decomposition with Gabor atoms adds to the approaches for the elimination of ringing noise. It especially allows the separation of signal and ringing of the cable and effectively stabilizes data interpretation even if those are superimposed. This finally increases the resolution and helps to assess

small-scale effects during exploration, not only for geothermal energy.

DATA AVAILABILITY STATEMENT

Data will be made available after the projects embargo period via the GFZ repository (dataservices.gfz-potsdam.de/portal).

ACKNOWLEDGEMENTS

The research project RissDom-A is funded by the German Federal Ministry of Economic Affairs and Energy (grant 0324065). We would like to thank all contractors involved in acquisition and processing and to acknowledge Ernst Huenges for the establishment of research activities at the Groß Schönebeck in-situ geothermal laboratory. Additionally, the authors thank the editor Dr Noalwenn Dubos-Sallée, the associate editor Hervé Chauris and three anonymous reviewers for their comments and suggestions that helped to improve the paper.

ORCID

Evgeniia Martuganova https://orcid.org/0000-0003-4261-074X
Klaus Bauer https://orcid.org/0000-0002-7777-2653
Jan Henninges https://orcid.org/0000-0003-2043-6947
Charlotte M. Krawczyk https://orcid.org/0000-0002-5505-6293

REFERENCES

Ahmed, F.Y. (2012) Gas detection using matching pursuit spectral decomposition seismic attribute. *74th EAGE Conference and Exhibition incorporating EUROPEC 2012*, Copenhagen, Denmark. Expanded Abstracts, P155. https://doi.org/10.3997/2214-4609.20148530.

Backus, M.M. (1959) Water reverberations – their nature and elimination. *Geophysics*, 24, 233–261. https://doi.org/10.1190/1.1438579.

Bakku, S.K., Fehler, M., Wills, P., Mestayer, J., Mateeva, A. and Lopez, J. (2014) Vertical seismic profiling using distributed acoustic sensing in a hydrofrac treatment well. *84th SEG Annual Meeting*, Denver, Colorado, USA. Expanded Abstract, 5024–5028. https://doi.org/10.1190/segam2014-1559.1.

Barberan, C., Allanic, C., Avila, D., Hy-Billiot, J., Hartog, A., Frignet, B. *et al.* (2012) Multi-offset seismic acquisition using optical fiber behind tubing. *74th EAGE Conference and Exhibition incorporating EUROPEC 2012*, Copenhagen, Denmark. Expanded Abstracts, Y003. https://doi.org/10.3997/2214-4609.20148798.

Bauer, K., Norden, B., Ivanova, A., Stiller, M. and Krawczyk, C.M. (2020) Wavelet transform-based seismic facies classification and modelling: application to a geothermal target horizon in the NE German Basin. *Geophysical Prospecting*, 68, 466–482. https://doi.org/10.1111/1365-2478.12853.

Borland, W., Hearn, R. and Sayed, A. (2016) Improving the acquisition efficiency of acquiring borehole seismic data by recording optical distributed acoustic data on a wireline hybrid electrooptical cable. *86th SEG Annual Meeting*, Dallas, Texas, USA. Expanded Abstracts, 800–804. https://doi.org/10.1190/segam2016-13951115.1.

Burg, J.P. (1972) The relationship between maximum entropy spectra and maximum likelihood spectra. *Geophysics*, 37, 375–376. https://doi.org/10.1190/1.1440265.

Burg, J.P. (1975) *Maximum Energy Spectral Analysis*. *PhD Thesis*, Stanford University.

Chang, H. and Nakata, N. (2020) Investigation of the time-lapse changes with the DAS borehole data at the Brady geothermal field using deconvolution interferometry. *SEG Technical Program Expanded Abstracts 2020*, pp. 3417–3421.

Chen, J., Ning, J., Chen, W., Wang, X., Wang, W. and Zhang, G. (2019) Distributed acoustic sensing coupling noise removal based on sparse optimization. *Interpretation*, 7(2), T373–T382. https://doi.org/10.1190/INT-2018-0080.1.

Chen, S., Li, Y. and Cheng, J. (2018) Ground roll attenuation applying matching pursuit algorithm. 80th EAGE Conference and Exhibition, Copenhagen, Denmark. Expanded Abstracts, TuP702. https://doi.org/10.3997/2214-4609.201800934.

Constantinou, A., Farahani, A., Cuny, T. and Hartog, A. (2016) Improving DAS acquisition by real-time monitoring of wireline cable coupling. *86th SEG Annual Meeting*, Dallas, Texas, USA. Expanded Abstracts, 5603–5607. https://doi.org/10.1190/segam2016-13950092.1.

Correa, J., Egorov, A., Tertyshnikov, K., Bona, A., Pevzner, R., Dean, T., *et al.* (2017) Analysis of signal to noise and directivity characteristics of DAS VSP at near and far offsets — A CO2CRC Otway Project data example. *The Leading Edge*, 36, 994a1–994a7. https://doi.org/10.1190/tle36120994a1.1.

Daley, T.M., Miller, D.E., Dodds, K., Cook, P. and Freifeld, B.M. (2016) Field testing of modular borehole monitoring with simultaneous distributed acoustic sensing and geophone vertical seismic profiles at Citronelle, Alabama. *Geophysical Prospecting*, 64, 1318–1334. http://doi.org/10.1111/1365-2478.12324.

Dean, T., Constantinou, A., Cuny, T., Frignet, B., Hartog, A., Kimura, T., *et al.* (2015) Vertical seismic profiles: now just another log? *85th SEG Annual Meeting*, New Orleans, Louisiana, USA. Expanded Abstracts, 5544–5548. https://doi.org/10.1190/segam2015-5804007.1.

Dean, T., Cuny, T. and Hartog, A.H. (2017) The effect of gauge length on axially incident P-waves measured using fibre optic distributed vibration sensing. *Geophysical Prospecting*, 65, 184–193. http://doi.org/10.1111/1365-2478.12419.

Didraga, C. (2015) DAS VSP recorded simultaneously in cemented and tubing installed fiber optic cables. *77th EAGE Conference and Exhibition*, Madrid, Spain. Expanded Abstracts, Tu N118 14. http://doi.org/10.3997/2214-4609.201412738.

Dou, S., Lindsey, N., Wagner, A., Daley, T., Freifeld, B., Robertson, M., *et al.* (2017) Distributed acoustic sensing for seismic monitoring of

the near surface: a traffic-noise interferometry case study. *Scientific Reports*, 7, 11620. https://doi.org/10.1038/s41598-017-11986-4.

Durka, P., Malinowska, U., Zieleniewska, M., O'Reilly, C., Różański, P. and Żygierewicz, J. (2015) Spindles in Svarog: framework and software for parametrization of EEG transients. *Frontiers in Human Neuroscience*, 9, 258. https://doi.org/10.3389/fnhum.2015.00258.

Elboth, T., Geoteam, F., Qaisrani, H.H. and Hertweck, T. (2008) Denoising seismic data in the time-frequency domain. *78th SEG Annual Meeting*, Las Vegas, Nevada, USA. Expanded Abstracts, 2622–2626. http://doi.org/10.1190/1.3063887.

Every, M.J., King, R. and Weaver, D.S. (1982) Vortex-excited vibrations of cylinders and cables and their suppression. *Ocean Engineering*, 9, 135–157. http://doi.org/10.1016/0029-8018(82)90010-5.

Götz, J., Lüth, S., Henninges, J. and Reinsch, T. (2018) Vertical seismic profiling using a daisy-chained deployment of fibre-optic cables in four wells simultaneously – case study at the Ketzin carbon dioxide storage site. *Geophysical Prospecting*, 66, 1201–1214. http://doi.org/10.1111/1365-2478.12638.

Grandi, S., Dean, M. and Tucker, O. (2017) Efficient containment monitoring with distributed acoustic sensing: feasibility studies for the former Peterhead CCS project. *Energy Procedia*, 114, 3889–3904. http://doi.org/10.1016/j.egypro.2017.03.1521.

Griffiths, L.J., Smolka, F.R. and Trembly, L.D. (1977) Adaptive deconvolution: a new technique for processing time-varying seismic data. *Geophysics*, 42, 742–759. http://doi.org/10.1190/1.1440743.

Hale, D., Widrow, B. and Stearns, S.D. (1985) *Adaptive Signal Processing*. Prentice-Hall.

Hartog, A., Frignet, B., Mackie, D. and Clark, M. (2014) Vertical seismic optical profiling on wireline logging cable. *Geophysical Prospecting*, 62, 693–701. http://doi.org/10.1111/1365-2478.12141.

Henninges, J., Baumann, G., Brandt, W., Cunow, C., Poser, M., Schrötter, J. *et al*. (2011) A novel hybrid wireline logging system for downhole monitoring of fluid injection and production in deep reservoirs. *73rd EAGE Conference & Exhibition*. http://doi.org/10.3997/2214-4609.20149727.

Henninges, J., Götz, J., Jousset, P., Lüth, S. and Reinsch, T. (2017) New methods in geophysical exploration and monitoring with DTS and DAS. *EAGE/DGG Workshop on Fibre Optic Technology in Geophysics*, Potsdam, Germany. Expanded Abstracts, FrSR07. https://doi.org/10.3997/2214-4609.201700156.

Henninges, J., Martuganova, E., Stiller, M., Norden, B. and Krawczyk, C.M. (2021) Wireline distributed acoustic sensing allows 4.2 km deep vertical seismic profiling of the Rotliegend 150°C geothermal reservoir in the North German Basin. *Solid Earth*, 12, 521–537. https://doi.org/10.5194/se-12-521-2021.

Jousset, P., Reinsch, T., Ryberg, T., Blanck, H., Clarke, A., Aghayev, R., *et al*. (2018) Dynamic strain determination using fibre-optic cables allows imaging of seismological and structural features. *Nature Communications*, 9, 2509. https://doi.org/10.1038/s41467-018-04860-y.

Kobayashi, Y., Uematsu, Y., Mochiji, S. and Xue, Z. (2020) A field experiment of walkaway distributed acoustic sensing vertical seismic profile in a deep and deviated onshore well in Japan using a fibre optic cable deployed inside coiled tubing. *Geophysical Prospecting*, 68, 501–520. https://doi.org/10.1111/1365-2478.12863.

Krawczyk, C.M., Stiller, M., Bauer, K., Norden, B., Henninges, J., Ivanova, A. *et al*. (2019) 3-D seismic exploration across the deep geothermal research platform Groß Schönebeck north of Berlin/Germany. *Geothermal Energy*, 7, 15. https://doi.org/10.1186/s40517-019-0131-x.

Krischer, L., Megies, T., Barsch, R., Beyreuther, M., Lecocq, T., Caudron, C. *et al*. (2015) ObsPy: a bridge for seismology into the scientific Python ecosystem. *Computational Science & Discovery*, 8, 014003. https://doi.org/10.1088/1749-4699/8/1/014003.

Kuś, R., Różański, P.T. and Durka, P.J. (2013) Multivariate matching pursuit in optimal Gabor dictionaries: theory and software with interface for EEG/MEG via Svarog. *BioMedical Engineering OnLine*, 12, 94. https://doi.org/10.1186/1475-925X-12-94.

Mallat, S.G. and Zhang, Z. (1993) Matching pursuits with time-frequency dictionaries. *IEEE Transactions on Signal Processing*, 41, 3397–3415. http://doi.org/10.1109/78.258082.

Mateeva, A., Lopez, J., Potters, H., Mestayer, J., Cox, B., Kiyashchenko, D., *et al*. (2014) Distributed acoustic sensing for reservoir monitoring with vertical seismic profiling. *Geophysical Prospecting*, 62, 679–692. https://doi.org/10.1111/1365-2478.12116.

Miller, D., Parker, T., Kashikar, S., Todorov, M. and Bostick, T. (2012) Vertical seismic profiling using a fibre-optic cable as a distributed acoustic sensor. *74th EAGE Conference and Exhibition incorporating EUROPEC 2012*, Copenhagen, Denmark. Expanded Abstracts, Y004. https://doi.org/10.3997/2214-4609.20148799.

Mondanos, M. and Coleman, T. (2019) Application of distributed fibre-optic sensing to geothermal reservoir characterization and monitoring. *First Break*, 37, 51–56. https://doi.org/10.3997/1365-2397.n0040.

Munn, J., Coleman, T., Parker, B., Mondanos, M. and Chalari, A. (2017) Novel cable coupling technique for improved shallow distributed acoustic sensor VSPs. *Journal of Applied Geophysics*, 138, 72–79. https://doi.org/10.1016/j.jappgeo.2017.01.007.

Naldrett, G., Parker, T., Shatalin, S., Mondanos, M. and Farhadiroushan, M. (2020) High-resolution Carina distributed acoustic fibreoptic sensor for permanent reservoir monitoring and extending the reach into subsea fields. *First Break*, 38, 71–76. https://doi.org/10.3997/1365-2397.fb2020012.

Niedzwecki, J. and Fang, S.M. (2013) Suppression of flow-induced vibrations using ribbon fairings. *International Journal of Computational Methods and Experimental Measurements*, 1, 395–405. https://doi.org/10.2495/CMEM-V1-N4-395-405.

Ozbek, A., Özdemir, A.K. and Vassallo, M. (2008) Interpolation of irregularly sampled data by matching pursuit. *70th EAGE Conference and Exhibition incorporating SPE EUROPEC*. Rome, Italy. Expanded Abstracts, G025. https://doi.org/10.3997/2214-4609.20147734.

Raisutis, R., Kazys, R., Mazeika, L., Samaitis, V. and Zukauskas, E. (2016) Propagation of ultrasonic guided waves in composite multi-wire ropes. *Materials*, 9, 451. https://doi.org/10.3390/ma9060451.

Schilke, S., Donno, D., Chauris, H., Hartog, A., Farahani, A. and Pico, Y. (2016) Numerical evaluation of sensor coupling of distributed acoustic sensing systems in vertical seismic profiling. *86th SEG Annual Meeting*, Dallas, Texas, USA. Expanded Abstracts, 677–681. https://doi.org/10.1190/segam2016-13527500.1.

Schilke, S., Donno, D., Hartog, A.H. and Chauris, H. (2017) DAS and its coupling for VSP applications using wireline cable. *EAGE/DGG Workshop on Fibre Optic Technology in Geophysics*, Potsdam, Germany. Expanded Abstracts, FrSR09. https://doi.org/10.3997/2214-4609.201700158.

Semnani, A., Wang, L., Ostadhassan, M., Nabi-Bidhendi, M. and Araabi, B.N. (2019) Time-frequency decomposition of seismic signals via quantum swarm evolutionary matching pursuit. *Geophysical Prospecting*, 67, 1701–1719. https://doi.org/10.1111/1365-2478.12767.

Song, J.-G., Gong, Y.-L. and Li, S. (2015) High-resolution frequency-domain Radon transform and variable-depth streamer data deghosting. *Applied Geophysics*, 12, 564–572. https://doi.org/10.1007/s11770-015-0525-x.

Stiller, M., Krawczyk, C.M., Bauer, K., Henninges, J., Norden, B., Huenges, E. and Spalek, A. (2018) 3D-Seismik am Geothermieforschungsstandort Groß Schönebeck. *BBR - Fachmagazin für Brunnen- und Leitungsbau*, 1, 84–91.

The ObsPy Development Team (2017) ObsPy 1.1.0. https://zenodo.org/record/165135https:/doi.org/10.5281/ZENODO.165135

The Svarog developers team (2014) BrainTech/matching-pursuit. https://github.com/BrainTech/matching-pursuit

The Svarog developers team (2016) BrainTech/svarog. https://github.com/BrainTech/svarog

Wang, P., Nimsaila, K., Zhuang, D., Fu, Z., Shen, H., Poole, G. and Chazalnoel, N. (2015) Joint 3D source-side deghosting and designature for modern air-gun arrays. *77th EAGE Annual Meeting*, Madrid, Spain. Expanded Abstracts, Th N103 10. https://doi.org/10.3997/2214-4609.201413190.

Wang, Y. (2010) Multichannel matching pursuit for seismic trace decomposition. *Geophysics*, 75(4), V61–V66. https://doi.org/10.1190/1.3462015.

Waskom, M., Botvinnik, O., O'Kane, D., Hobson, P., Lukauskas, S., Gemperline, D.C., *et al.* (2017) mwaskom/seaborn: v0.8.1. https://zenodo.org/record/883859https:/doi.org/10.5281/ZENODO.883859

Wawrzyniak, K. (2006) Analysis of acoustic full waveforms based on matching pursuit parameterization. *68th EAGE Conference and Exhibition incorporating SPE EUROPEC*, Vienna, Austria. Expanded Abstracts, P206. https://doi.org/10.3997/2214-4609.201402445.

Willis, M., Palacios, W., Ellmauthaler, A. and Zhao, X. (2020) Mitigation of zigzag noise on DAS VSP records acquired in vertical wells. 82nd EAGE Conference & Exhibition, online, 1–5, Th_Dome3_11. https://doi.org/10.3997/2214-4609.202011089.

Willis, M.E., Wu, X., Palacios, W. and Ellmauthaler, A. (2019) Understanding cable coupling artifacts in wireline-deployed DAS VSP data. *89th SEG Annual Meeting*, San Antonio, Texas, USA. Expanded Abstracts, 5310–5314. https://doi.org/10.1190/segam2019-3208294.1.

Yu, G., Cai, Z., Chen, Y., Wang, X., Zhang, Q., Li, Y., *et al.* (2016a) Walkaway VSP using multimode optical fibers in a hybrid wireline. *The Leading Edge*, 35, 615–619. http://doi.org/10.1190/tle35070615.1.

Yu, G., Chen, Y.Z., Wang, X.M., Zhang, Q.H., Li, Y.P., Zhao, B.Y., *et al.* (2016b) Walkaway VSP using multimode optical fibres in a hybrid wireline. *78th EAGE Conference and Exhibition 2016*, Vienna, Austria. Expanded Abstracts, Th_STZ2_05. https://doi.org/10.3997/2214-4609.201601602.

Zimmermann, G., Moeck, I. and Blöcher, G. (2010) Cyclic waterfrac stimulation to develop an enhanced geothermal system (EGS)—conceptual design and experimental results. *Geothermics*, 39, 59–69. https://doi.org/10.1016/j.geothermics.2009.10.003.

